



RESEARCH MEMORANDUM

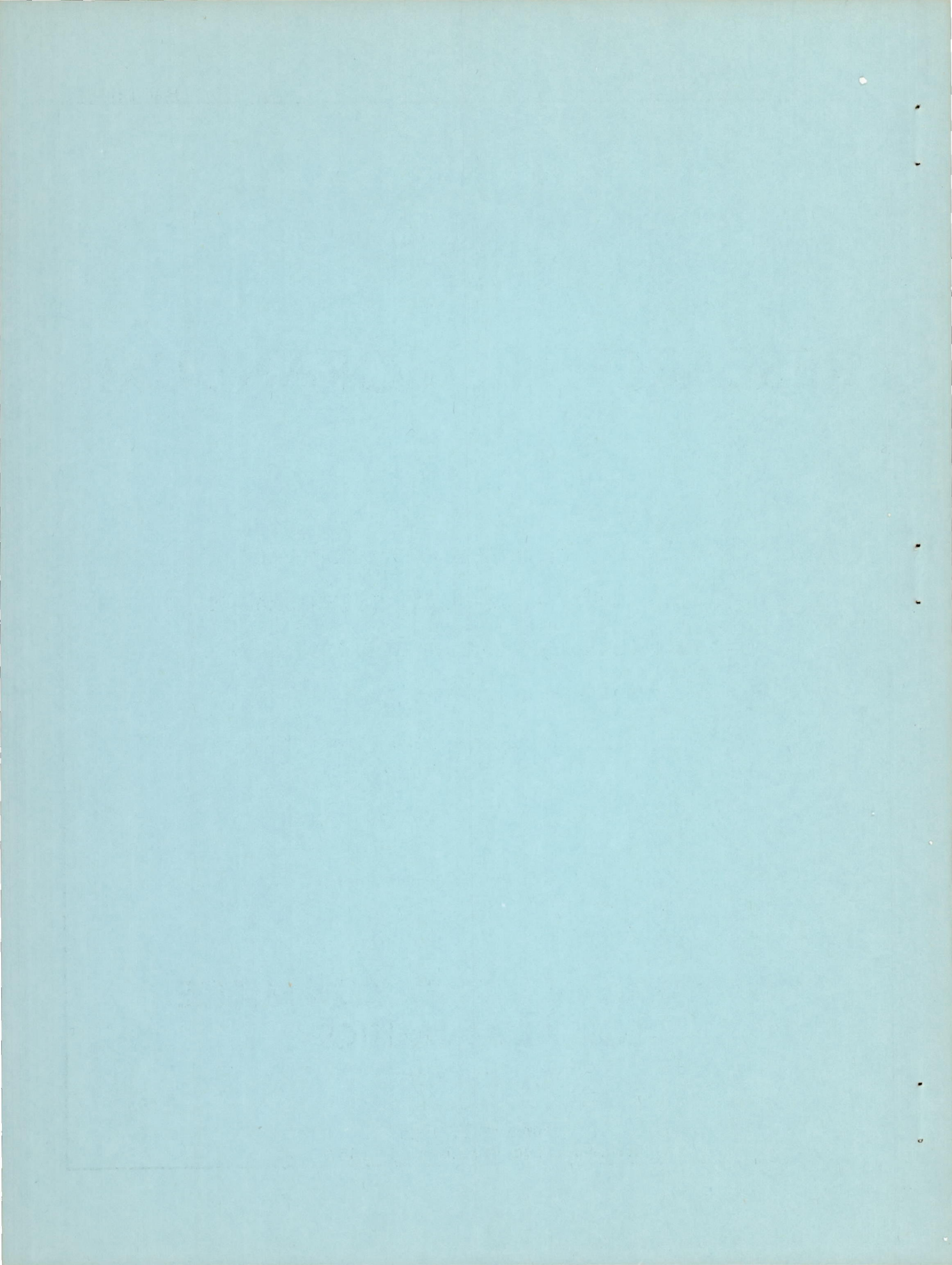
LONGITUDINAL STABILITY INVESTIGATION FOR A MACH NUMBER
RANGE OF 0.8 TO 1.7 OF AN AIRPLANE CONFIGURATION WITH
A 45° SWEPT WING AND A LOW HORIZONTAL TAIL

By John C. McFall, Jr.

Langley Aeronautical Laboratory
Langley Field, Va.

NATIONAL ADVISORY COMMITTEE
FOR AERONAUTICS
WASHINGTON

February 8, 1956
Declassified December 13, 1957



NATIONAL ADVISORY COMMITTEE FOR AERONAUTICS

RESEARCH MEMORANDUM

LONGITUDINAL STABILITY INVESTIGATION FOR A MACH NUMBER
RANGE OF 0.8 TO 1.7 OF AN AIRPLANE CONFIGURATION WITH
A 45° SWEPT WING AND A LOW HORIZONTAL TAIL

By John C. McFall, Jr.

SUMMARY

An airplane configuration model having a 45° swept wing of aspect ratio 4.0 and taper ratio of 0.3 with a low swept horizontal tail has been flown in a longitudinal stability investigation over a Mach number range of 0.8 to 1.7. Longitudinal aerodynamic coefficients and stability derivatives for the configuration are presented as functions of Mach number over the test range. Comparisons of lift-curve slopes are made with wind-tunnel data and comparisons of tail effectiveness are made with rocket-model data, and show generally good agreement. Absence of an unstable break in the pitching-moment curve, usually associated with this wing, indicates a favorable location of the horizontal tail for the lift and Mach number range of the investigation.

INTRODUCTION

With the advent of transonic airplanes the need for aerodynamic derivatives at higher Mach numbers than generally available has greatly increased. Some earlier investigations at transonic and low supersonic speeds to determine longitudinal and lateral stability characteristics of airplane configurations having wings of various plan forms and thickness have been reported by the NACA in references 1 to 7. More recently, the flight tests reported in references 8 to 11 have extended the investigation of airplane configurations to higher supersonic Mach numbers (1.7 to 2.3). As a continuation of this general research free-flight program, an airplane configuration with a 45° swept wing of aspect ratio 4.0 and a low horizontal tail has been flown in a longitudinal stability investigation over a Mach number range of 0.8 to 1.7. Data from the present test are compared with other rocket-model data, reference 9, and with wind-tunnel data, references 12 to 16. The model was flown at the Langley Pilotless Aircraft Research Station at Wallops Island, Va.

SYMBOLS

C_N	normal-force coefficient, $\frac{a_n}{g} \frac{W/S}{q}$
C_C	chord-force coefficient, $-\frac{a_l}{g} \frac{W/S}{q}$
C_L	lift coefficient, $C_N \cos \alpha - C_C \sin \alpha$
$C_{L\alpha}$	lift-curve slope, per deg
$C_{L\delta}$	effectiveness of horizontal tail in producing lift, per deg
C_D	drag coefficient, $C_C \cos \alpha + C_N \sin \alpha$
C_m	pitching-moment coefficient, center of gravity located at $0.272\bar{c}$
$C_{m\alpha}$	slope of pitching-moment curve, per deg
$C_{m\delta}$	effectiveness of horizontal tail in producing pitching moment, per deg
$C_{n\beta}^*$	effective value of $C_{n\beta}$, $C_{n\beta}^* = 0.688 \frac{I_z}{q S b P^2}$, per deg
$C_{n\beta}$	rate of change of yawing-moment coefficient with side slip angle, per deg
$C_{m_q} + C_{m\dot{\alpha}}$	sum of pitch-damping coefficients, per radian, $57.3 \left[\frac{\partial C_m}{\partial (\frac{q\bar{c}}{2V})} + \frac{\partial C_m}{\partial (\frac{\dot{\alpha}\bar{c}}{2V})} \right]$
A	aspect ratio
a_l	longitudinal acceleration, ft/sec^2
a_n	normal acceleration, ft/sec^2
a.c.	aerodynamic center
b	wing span, ft
cps	cycles per second

\bar{c}	mean aerodynamic chord, ft
F	fuselage
g	acceleration of gravity, ft/sec ²
I_Z	moment of inertia in yaw, slug-ft ²
K	factor for converting elastic wing-lift data to rigid values
L	load applied, lb; or lift, lb
D	drag, lb
M	Mach number
T	tail
P	period of oscillation, sec
p	free-stream static pressure, lb/sq ft
p_0	standard sea-level static pressure (2,116 lb/sq ft)
q	free-stream dynamic pressure, lb/sq ft; or $\frac{d\theta}{dt}$
R	Reynolds number, based on wing mean aerodynamic chord
S	wing area (including area enclosed within fuselage), sq ft
$T_{1/2}$	time to damp to one-half amplitude, sec
t	time, sec
W	weight, lb; or wing
y	lateral distance from fuselage center line, ft
α	angle of attack, deg
$\dot{\alpha} = \frac{d\alpha}{dt}$	
β	angle of sideslip, deg
δ	control surface deflection with respect to fuselage center line (parallel to free stream), deg

η loading station or twist station, $\frac{y}{b/2}$

θ local streamwise wing twist angle produced by load L , radians; or model angle of pitch, deg

Subscript:

t trim, or tail

The symbols α and δ used as subscripts indicate the derivative of the quantity with respect to the subscript, for example,

$$C_{L\alpha} = \frac{\partial C_L}{\partial \alpha}$$

MODEL AND GROUND TESTS

Model

Physical characteristics of the model are shown in figure 1 by a drawing and in figures 2(a) and 2(b) by photographs. A photograph of the boost system utilized along with the model in launching position is presented as figure 2(c). The holes in the fuselage, figures 2(a) and 2(b), were plugged and faired before the model was flown.

The fuselage and empennage of this configuration are the same as those of reference 9, with two exceptions: the vertical fin was changed from a composite of wood and aluminum alloy to solid aluminum alloy, and the section of the fuselage in which the wing was mounted was changed from aluminum alloy to steel. The fuselage ordinates of the present model are presented as table I.

The wing of the present configuration had an aspect ratio of 4.0, 45° sweepback of the quarter-chord line, taper ratio of 0.3, and NACA 65A006 airfoil sections parallel to the free stream. The wing was made of solid steel.

The horizontal tail was deflected in an approximate square-wave program from $\delta = 0^\circ$ to $\delta = -4.5^\circ$ by an electrohydraulic system described in reference 5.

The range of the angle-of-attack indicator was limited to $\pm 15^\circ$. The sting holding the indicator was deflected to allow angle-of-attack measurements from -3.3° to 26.7° .

The model weighed 151.3 pounds and had the following moments of inertia: pitch, 8.85 slug-ft²; yaw, 9.07 slug-ft²; roll, 1.08 slug-ft². The center of gravity of the model was located at the same longitudinal station as the 27.2-percent position of the wing mean aerodynamic chord.

Ground Tests

Vibrational characteristics of the model were determined by recording the response of the model to vibrations of known frequencies. These vibrations were applied with an electromechanical shaker. The observations were as follows:

Component	Frequency, cps
Wing: First bending	68
Second bending	224
Horizontal fins: First bending	92
Vertical Fin: First bending	52

Structural influence coefficients for the steel wing were measured as in reference 4 and are presented as figure 3. Measurements were made of instrument positions relative to the center of gravity of the model for later use in instrument displacement corrections to the data.

FLIGHT TEST AND INSTRUMENTATION

The model was launched at an angle of approximately 70° from the horizontal. Acceleration of the model to a Mach number of about 1.7 was accomplished with a solid-propellant rocket-boost system. The model separated from the booster at peak Mach number and data were recorded from the model throughout the 90 seconds of flight.

Most of the data presented were taken during the time from 3 to 20 seconds, while the model decelerated in coasting flight from $M = 1.7$ to $M = 0.8$. Some additional data (C_{L_a} at $M = 0.71$) are presented which were obtained during the last 20 seconds of the flight (70 to 90 seconds), while the model maintained a Mach number of approximately 0.73 after accelerating from a minimum Mach number of about 0.4 at the peak of the model flight path.

Instrumentation mounted in the model included the following: two normal accelerometers, transverse accelerometer, longitudinal accelerometer, angle-of-attack and sideslip indicator, control position indicator, angular accelerometer sensitive to roll, total pressure, and body orifice pressure.

Ground instrumentation included tracking radar, Doppler radar for velocity measurement, radiosonde for atmospheric conditions, telemeter receiving and recording equipment, and photographic tracking.

Reynolds number based on wing mean aerodynamic chord is shown in figure 4 for the Mach number range of the test.

The ratio of free-stream static pressure to standard sea-level pressure is presented as figure 5 for use in comparing the aeroelastic data of this test with data from other sources.

ANALYSIS

The analysis of the response of the model to the deflection of the all-movable horizontal tail in an approximate square-wave program followed the technique of reference 1. Small corrections for instrument displacements were applied to the accelerometers and to the angle-of-attack and sideslip vane as has been done in previous models, references 1 to 7.

ACCURACY

Estimated accuracies of basic quantities and calculated accuracy of parameters are presented as tables II and III. Estimated accuracies are based on experimental repeatability for weight and on the assumption of ± 1 -percent to ± 2 -percent error in full-scale instrument range. Mach numbers are thought to be accurate to ± 1 percent at supersonic speeds and ± 2 percent at subsonic speeds. As stated in reference 8, the incremental values and relative trends are much more accurate than the absolute level of the measurements. A comparison of $C_{I\alpha}$ and $C_{m\alpha}$ near the beginning of the flight after the model had decelerated to $M = 0.73$ with data obtained over the last 20 seconds of flight, also at approximately $M = 0.73$, indicated good repeatability in quantity as well as in measured slopes.

DISCUSSION OF RESULTS

Trim

Variation of trim angle of attack and trim lift coefficient with Mach number are shown in figure 6. The model trimmed at small negative angles of attack and low negative lift coefficients for the zero tail settings. For the -4.5° tail setting, trim angle of attack varied between 3° and 4° while trim lift coefficient varied between 0.17 and 0.30. A small amplitude oscillation in angle of sideslip of less than $\pm 1^\circ$ at supersonic speeds and less than $\pm 2^\circ$ at subsonic speeds trimmed about zero throughout the flight.

Lift

The linear variation of lift coefficient with angle of attack up to $\alpha = 8^\circ$ and $C_L = 0.5$ may be seen in figure 7.

Values of a factor K to correct measured lift-curve slopes to rigid values are shown in figure 8(a). These values were obtained from the structural influence coefficients of figure 3, using the method of reference 4. The 0.25-chord loading values were used up to $M = 1.0$, then the 0.50-chord loadings were used for the remainder of the test range.

The small K-factor correction for wing flexibility has been applied to the measured lift-curve slopes shown in figure 8(b) for the present test, and the comparison data presented from references 14, 15, and 16 are for rigid wings with reference 16 having been corrected to rigid values using data from reference 15. The solid curve shown in figure 8(b) was obtained by subtracting a value of tail contribution to total lift curve from the total lift-curve slope. This tail contribution was calculated from a similar plan-form lift-curve slope, obtained from references 4 and 14, with downwash values from reference 13. The agreement observed between present test values and data from other sources is considered good.

Drag

Drag coefficient as a function of lift coefficient for some of the test Mach numbers is shown in figure 9. Minimum drag values read directly from the low lift drag polars, and values extrapolated from the high lift polars, over their linear lift range, are presented in figure 10.

The drag-due-to-lift parameter dC_D/dC_L^2 plotted against Mach number is shown in figure 11. Values for zero leading-edge suction $\frac{1}{57.3C_{L\alpha}}$ are presented for comparison purposes.

The measured and extrapolated maximum lift-drag ratios are plotted as a function of Mach number in figure 12 and corresponding values of C_L for $(L/D)_{max}$ are presented in figure 13.

Static Longitudinal Stability

Variation of pitching moment with lift coefficient for several Mach numbers is shown in figure 14. In general, a linear variation of the pitching-moment curve is evident, although near-neutral stability was experienced by the configuration for the low Mach number oscillations at $M = 0.92$ and 0.84 for a lift coefficient of about 0.6 . A similar model (ref. 4) with an aspect-ratio-4 steel wing, but having a horizontal tail position about $0.5b/2$ above the wing chord plane extended, experienced a pitch-up maneuver to high angles of attack which was so violent that the model was not able to recover. This maneuver began at about the same value of lift coefficient at which the present model experienced near-neutral stability.

Values of period from the pitch oscillations are shown in figure 15 and converted to $C_{m\alpha}$ in figure 16. Variation of aerodynamic-center position with Mach number is presented in figure 17. These values were obtained using measured $C_{L\alpha}$ with $C_{m\alpha}$ from pitch-oscillation periods and also from measured values of C_m plotted against C_L in figure 14. The disagreement in aerodynamic-center position from the two methods, as much as 12 percent \bar{c} , may be caused by some moderate random lateral motions of the model which, as indicated by some recent unpublished electronic analog computer (REAC) studies, can have a large effect on values determined from the period of the pitch oscillations.

The effect of wing flexibility on aerodynamic center was calculated by the method of reference 4 and was found to cause a forward movement of less than 1 percent at subsonic speeds and less than 2 percent at supersonic speeds. This increment was not applied to the data.

Tail Effectiveness

The effectiveness of the horizontal tail in producing lift and pitching moment is illustrated in figure 18 along with values from the test of a model with the same configuration tail, reference 9. These tail effectiveness values were determined by the method presented in reference 1.

Damping in Pitch

Time for the pitch oscillation to damp to one-half amplitude plotted against Mach number is presented in figure 19. The sum of the pitch-damping coefficients ($C_{m_q} + C_{m_\alpha}$) in figure 20 shows considerable scatter, and is probably distorted by the small random lateral disturbance mentioned in the section on "Static Longitudinal Stability." The general level of pitch damping for this configuration is of the magnitude encountered by previous similar rocket models and indicates the high values of pitch-damping coefficient usually experienced near $M = 1.0$. A calculated value of tail pitch-damping coefficient is also shown in figure 20.

Static Directional Stability

Period values measured from oscillations in sideslip are shown in figure 21 and are converted to $C_{n_\beta}^*$ in figure 22 as in reference 12 and also as in reference 6 for other rocket models.

CONCLUDING REMARKS

Longitudinal aerodynamic coefficients and stability derivatives have been presented for an airplane configuration having a 45° swept wing of aspect ratio 4.0 and a low horizontal tail over a Mach number range of 0.8 to 1.7. Comparisons of lift-curve slopes measured in this investigation with wind-tunnel data and comparisons of tail effectiveness with other rocket-model data show good agreement. A linear variation of pitching-moment coefficient with lift coefficient was evidenced throughout the Mach number range of this test with the exception of the oscillations observed at a Mach number of 0.92 and 0.84 for a lift coefficient of about 0.6 where near-neutral stability was experienced by the model. Absence of an unstable break in the pitching-moment curve,

usually associated with this wing, indicates a favorable location of the horizontal tail for the range of lift coefficients and Mach numbers presented.

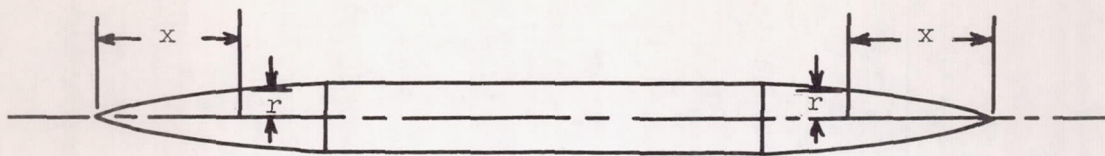
Langley Aeronautical Laboratory,
National Advisory Committee for Aeronautics,
Langley Field, Va., November 21, 1955.

REFERENCES

1. Gillis, Clarence L., Peck, Robert F., and Vitale, A. James: Preliminary Results From a Free-Flight Investigation at Transonic and Supersonic Speeds of the Longitudinal Stability and Control Characteristics of an Airplane Configuration With a Thin Straight Wing of Aspect Ratio 3. NACA RM L9K25a, 1950.
2. Gillis, Clarence L., and Vitale, A. James: Wing-On and Wing-Off Longitudinal Characteristics of an Airplane Configuration Having a Thin Unswept Tapered Wing of Aspect Ratio 3, as Obtained From Rocket-Propelled Models at Mach Numbers From 0.8 to 1.4. NACA RM L50K16, 1951.
3. Vitale, A. James, McFall, John C., Jr., and Morrow, John D.: Longitudinal Stability and Drag Characteristics at Mach Numbers From 0.75 to 1.5 of an Airplane Configuration Having a 60° Swept Wing of Aspect Ratio 2.24 as Obtained From Rocket-Propelled Models. NACA RM L51K06, 1952.
4. Vitale, A. James: Effects of Wing Elasticity on the Aerodynamic Characteristics of an Airplane Configuration Having 45° Sweptback Wings as Obtained From Free-Flight Rocket-Model Tests at Transonic Speeds. NACA RM L52L30, 1953.
5. McFall, John C., Jr.: Longitudinal Stability Characteristics at Transonic Speeds of a Rocket-Propelled Model of an Airplane Configuration Having a 45° Swept Wing of Aspect Ratio 6.0. NACA RM L53G22a, 1954.
6. Purser, Paul E., and Mitchell, Jesse L.: Miscellaneous Directional-Stability Data for Several Airplane-Like Configurations From Rocket-Model Tests at Transonic Speeds. NACA RM L52E06b, 1952.
7. Gillis, Clarence L., and Chapman, Rowe, Jr.: Summary of Pitch-Damping Derivatives of Complete Airplane and Missile Configurations as Measured in Flight at Transonic and Supersonic Speeds. NACA RM L52K20, 1953.
8. Peck, Robert F., and Coltrane, Lucille C.: Longitudinal Characteristics at Transonic and Supersonic Speeds of a Rocket-Propelled Airplane Model Having a 60° Delta Wing and a Low Swept Horizontal Tail. NACA RM L55F27, 1955.
9. Kehlet, Alan B.: Aerodynamic Characteristics at Transonic and Supersonic Speeds of a Rocket-Propelled Airplane Configuration Having a Diamond-Plan-Form Wing of Aspect Ratio 3.08 and a Low, Swept Horizontal Tail. NACA RM L54G27a, 1954.

10. Gillespie, Warren, Jr.: Lift, Drag, and Longitudinal Stability at Mach Numbers From 0.8 to 2.1 of a Rocket-Powered Model Having a Tapered Unswept Wing of Aspect Ratio 3 and Inline Tail Surfaces. NACA RM L55B10, 1955.
11. Gillespie, Warren, Jr.: Lift, Drag, and Longitudinal Stability at Mach Numbers From 1.4 to 2.3 of a Rocket-Powered Model Having a 52.5° Sweptback Wing of Aspect Ratio 3 and Inline Tail Surfaces. NACA RM L55I12, 1955.
12. Bishop, Robert C., and Lomax, Harvard: A Simplified Method for Determining From Flight Data the Rate of Change of Yawing-Moment Coefficient With Sideslip. NACA TN 1076, 1946.
13. Myers, Boyd C., II, and King, Thomas J., Jr.: Aerodynamic Characteristics of a Wing With Quarter-Chord Line Swept Back 45° , Aspect Ratio 4, Taper Ratio 0.3, and NACA 65A006 Airfoil Section - Transonic-Bump Method. NACA RM L9E25, 1949.
14. Delano, James B., and Mugler, John P., Jr.: Transonic Wind-Tunnel Investigation of the Effects of Taper Ratio and Body Indentation on the Aerodynamic Loading Characteristics of a 45° Sweptback Wing in the Presence of a Body. NACA RM L54L28, 1955.
15. King, Thomas J., Jr., and Pasteur, Thomas B., Jr.: Wind-Tunnel Investigation of the Aerodynamic Characteristics in Pitch of Wing-Fuselage Combinations at High Subsonic Speeds - Taper-Ratio Series. NACA RM L53E20, 1953.
16. Morrison, William D., Jr., and Alford, William J., Jr.: Effects of Horizontal-Tail Height and a Wing Leading-Edge Modification Consisting of a Full-Span Flap and a Partial-Span Chord-Extension on the Aerodynamic Characteristics in Pitch at High Subsonic Speeds of a Model With a 45° Sweptback Wing. NACA RM L53E06, 1953.

TABLE I.- FUSELAGE NOSE AND TAIL ORDINATES



x , in.	r , in.
0	0.168
.060	.182
.122	.210
.245	.224
.480	.294
.735	.350
1.225	.462
2.000	.639
2.450	.735
4.800	1.245
7.350	1.721
8.000	1.849
9.800	2.155
12.250	2.505
13.125	2.608
14.375	2.747
14.700	2.785
17.150	3.010
19.600	3.220
22.050	3.385
24.500	3.500

TABLE II.- ESTIMATED ACCURACIES OF BASIC QUANTITIES
 [Increments may be positive or negative]

M	W, percent	q, percent	$\frac{da_n}{d\alpha}$, percent	$\frac{a_l}{g}$ (1)	$\Delta\alpha$, percent (2)
1.7	1.5	3.8	2.0	0.1	2.0
1.3	1.5	4.8	2.0	.1	2.0
.9	1.5	5.7	2.0	.1	2.0

¹Obtained by assuming within ± 1 to 2 percent of full-scale instrument range.

² $\Delta\alpha$ is incremental change in α (that is, change in α due to change in δ).

TABLE III.- CALCULATED ACCURACY OF PARAMETERS
 [Increments may be positive or negative]

Increments in parameters due to estimated errors in -	$C_{L\alpha}$			$C_{D\min}$		$\Delta C_{L\text{trim}}$	
	M = 1.7	M = 1.3	M = 0.9	M = 1.7	M = 1.3	M = 1.7	M = 1.3
W	0.0008	0.0010	0.0014	0.0006	0.0006	0.0027	0.0035
q	.0020	.0034	.0052	.0016	.0019	.0068	.0110
$\frac{da_n}{d\alpha}$.0011	.0014	.0018	0	0	.0036	.0046
a_l	-----	-----	-----	.0014	.0036	.0002	.0004
$\Delta\alpha$	-----	-----	-----	-----	-----	.0036	.0046
Estimated error $\sqrt{\sum \text{Increments}^2}$.0024	.0038	.0057	.0022	.0041	.0089	.0132
Value of quantity	.0540	.070	.092	.042	.039	.180	.230
Estimated error in percent	4.44	5.43	6.20	5.23	10.50	4.94	5.74

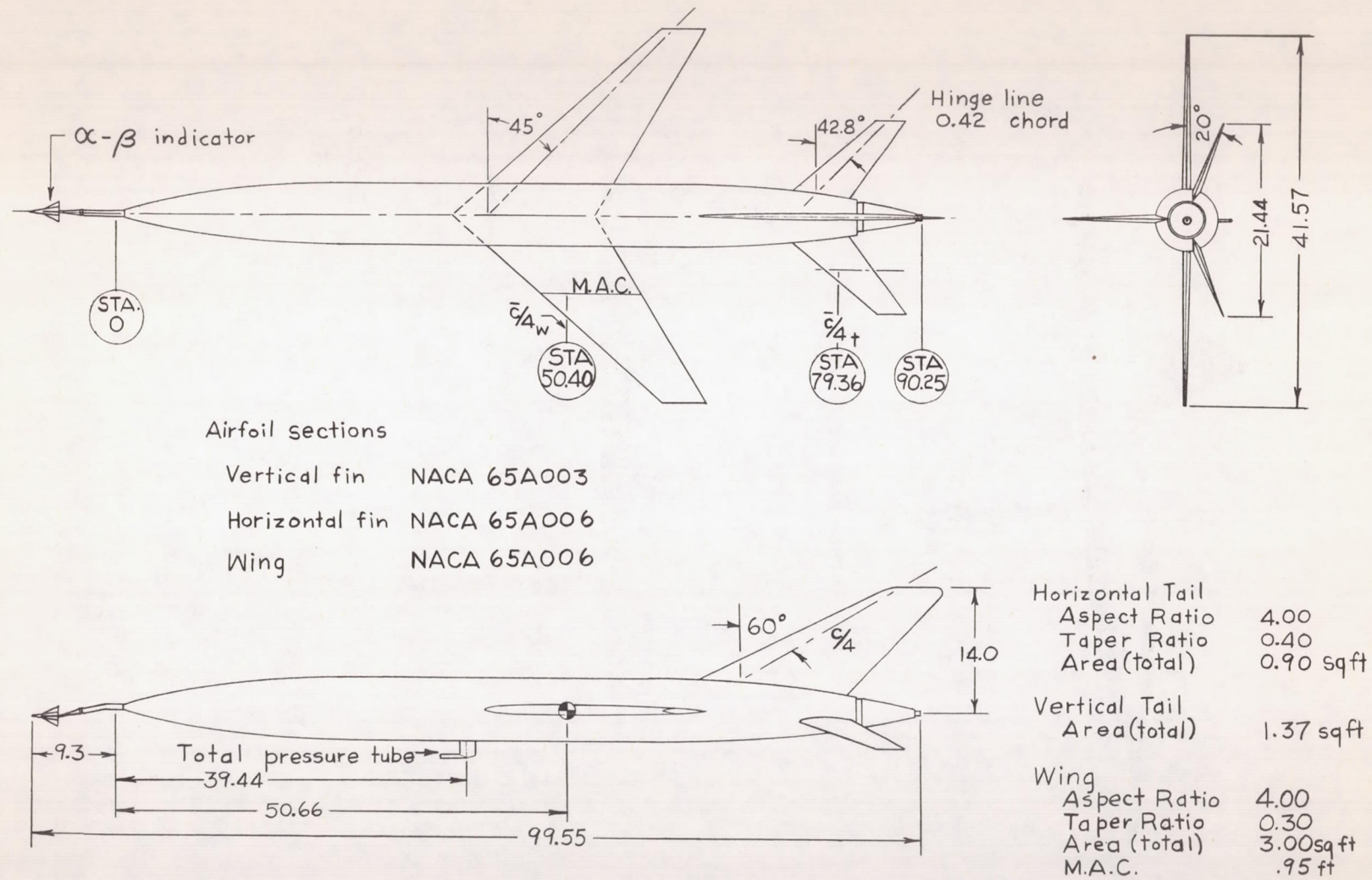
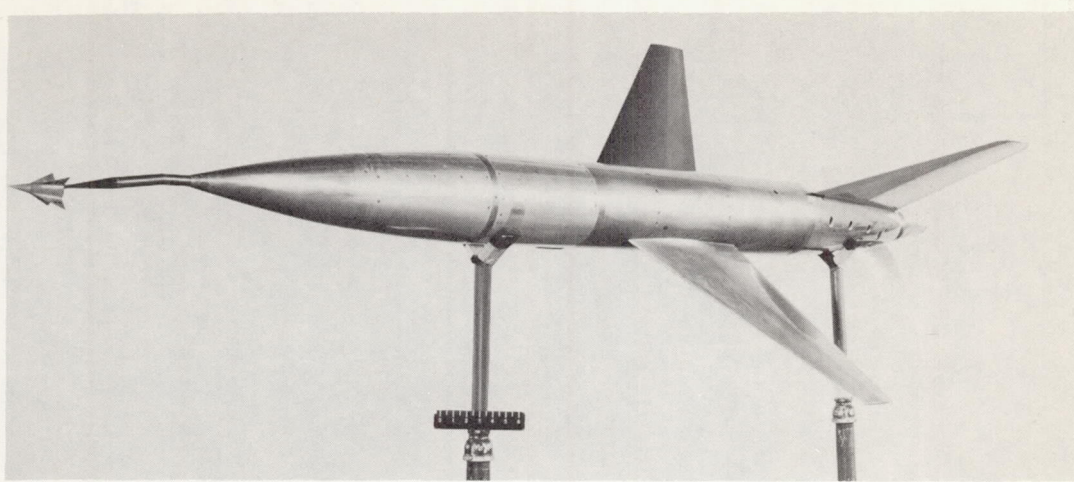
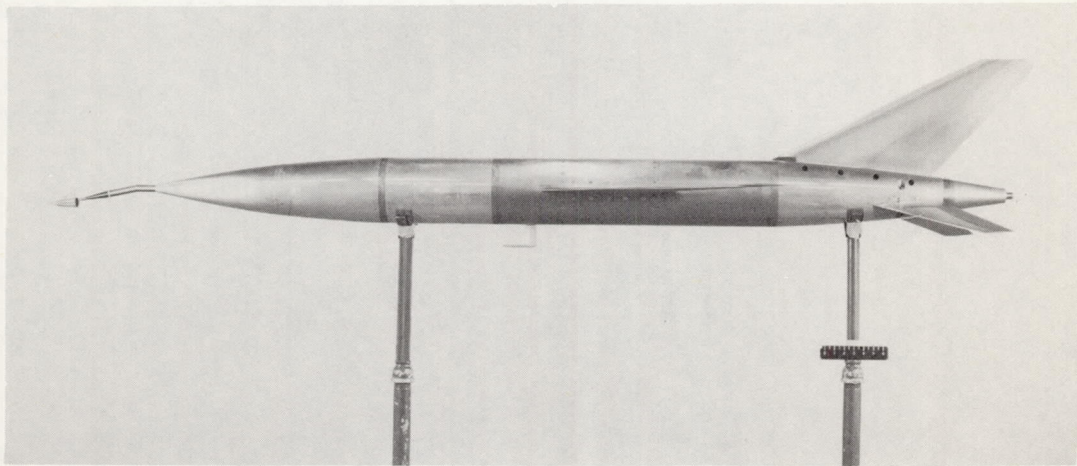


Figure 1.- Physical characteristics of model. All dimensions in inches.



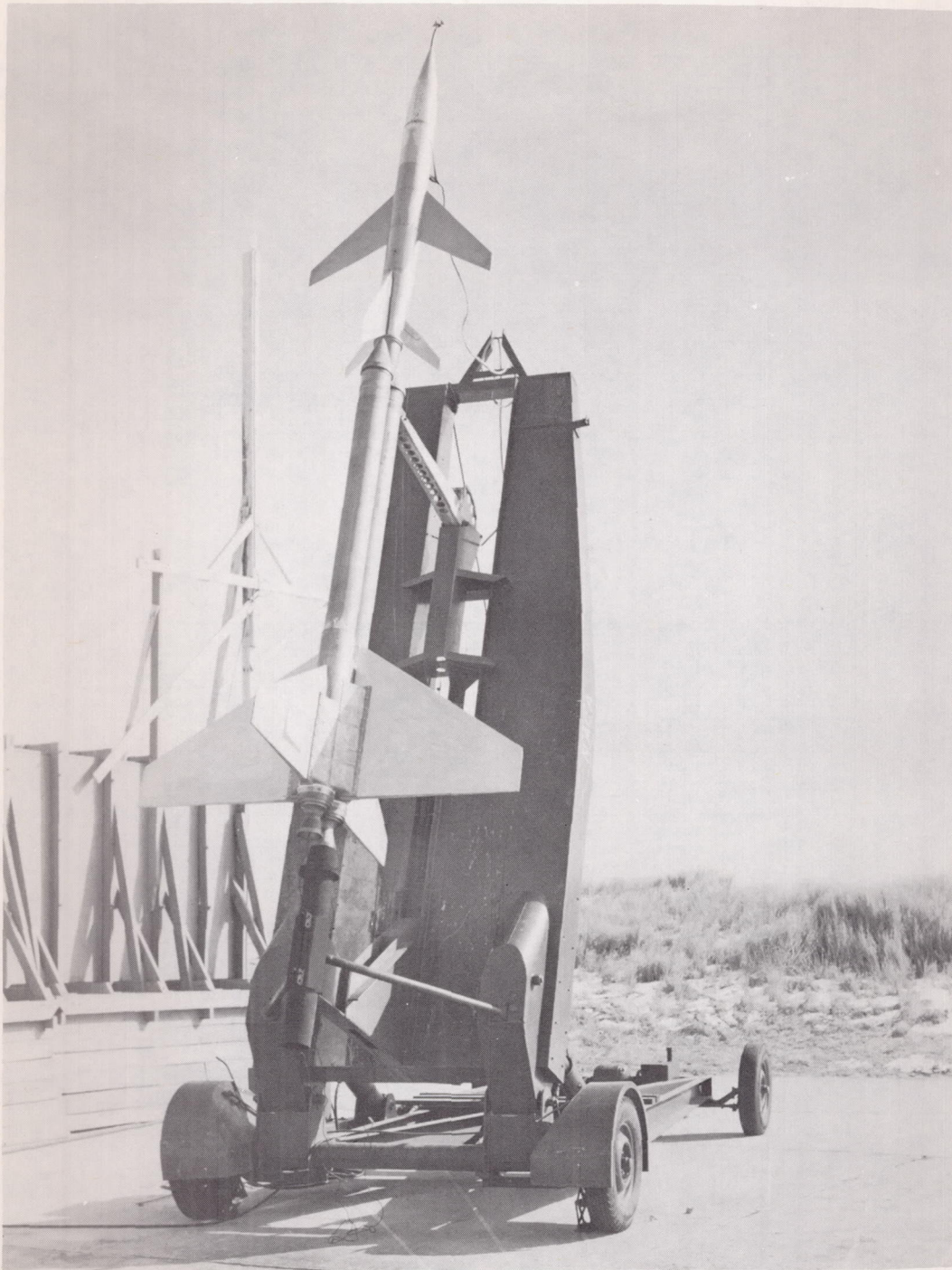
(a) Three-quarter front view.



(b) Side view.

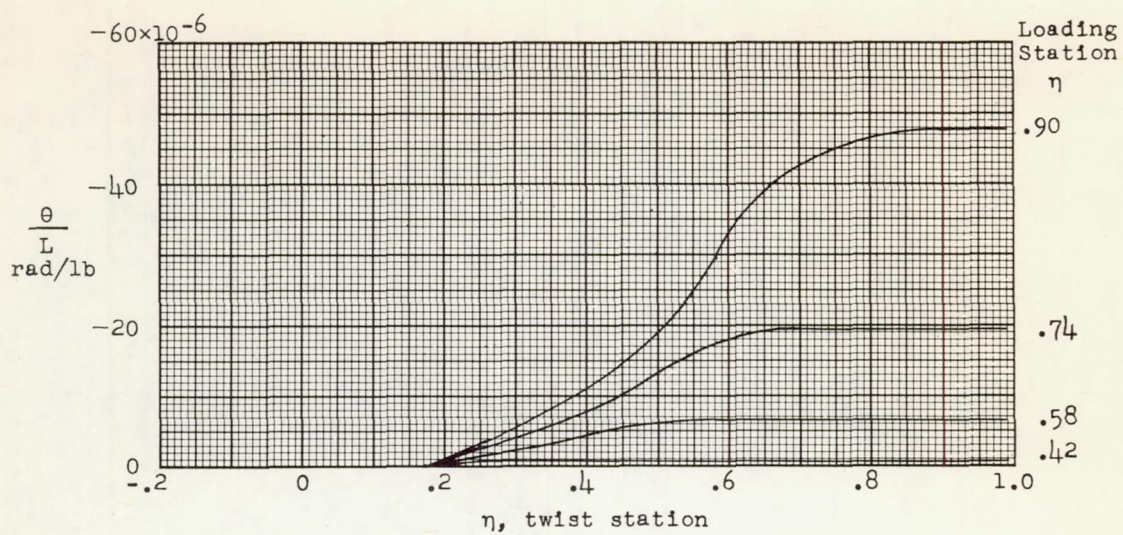
I-91677

Figure 2.- Photographs of model.

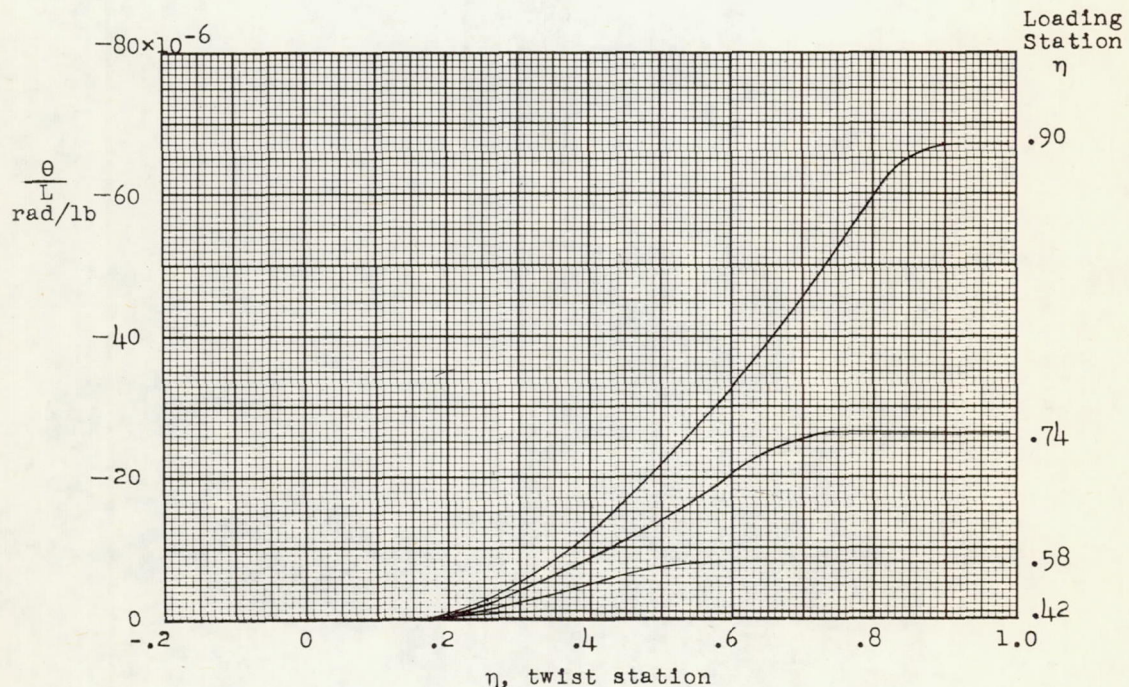


(c) Model on booster in launching position. **L-88160.1**

Figure 2.- Concluded.



(a) Loaded along 0.25-chord line.



(b) Loaded along 0.50-chord line.

Figure 3.- Twist in the free-stream direction per unit load applied at various stations along wing span.

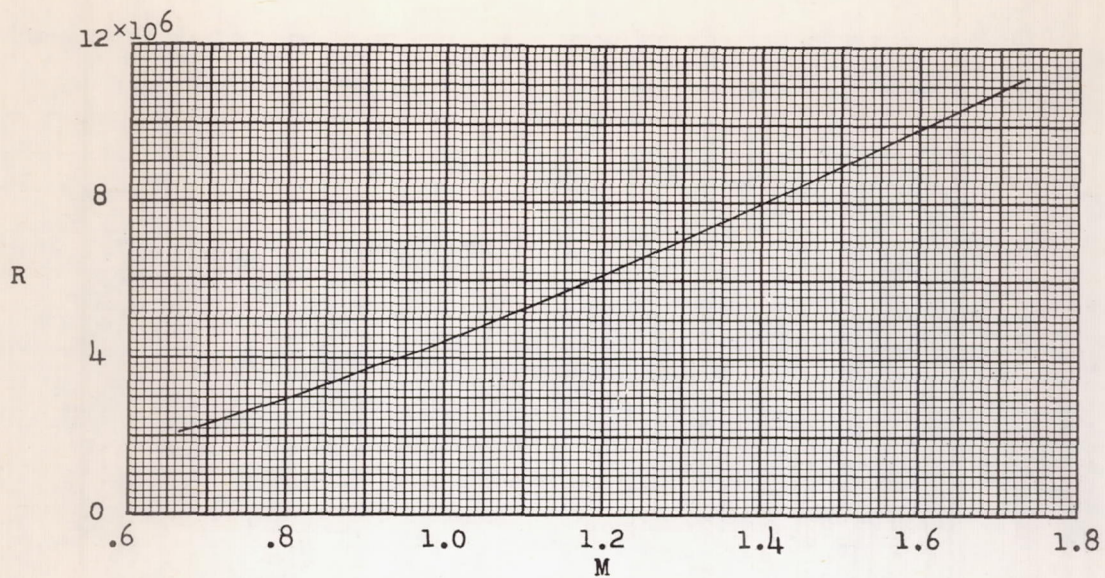


Figure 4.- Variation of test Reynolds number, based on wing mean aerodynamic chord, with Mach number.

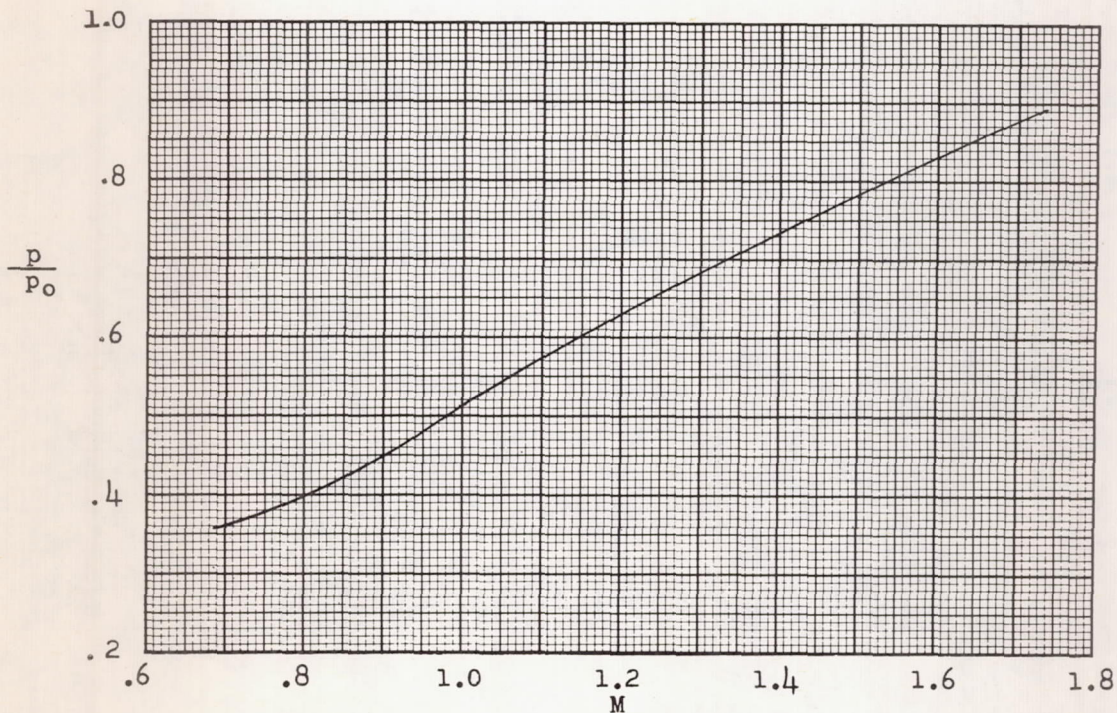
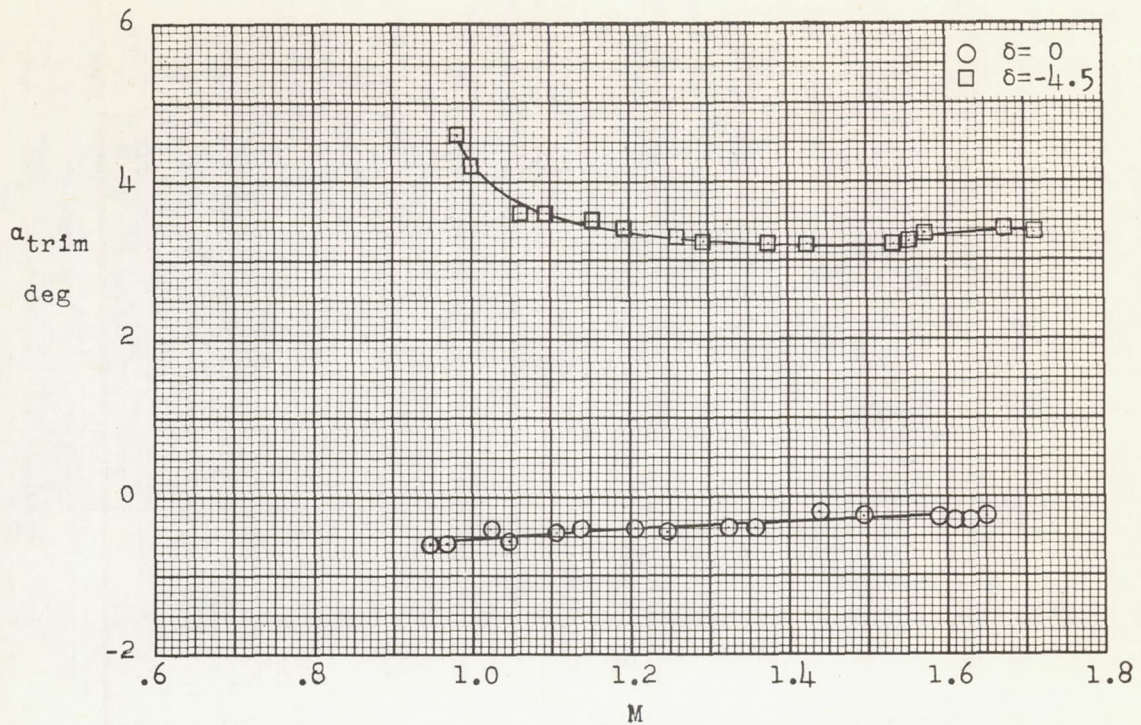
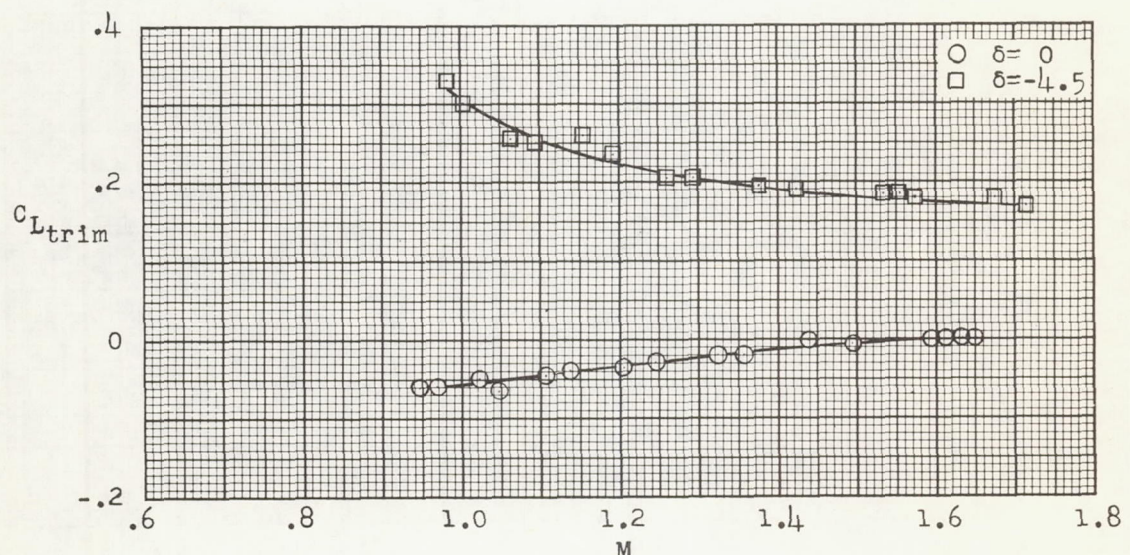


Figure 5.- Variation of ratio of free-stream static pressure to standard sea-level pressure with Mach number.



(a) Trim angle of attack.



(b) Trim lift coefficient.

Figure 6.- Variation of trim angle of attack and trim lift coefficient with Mach number.

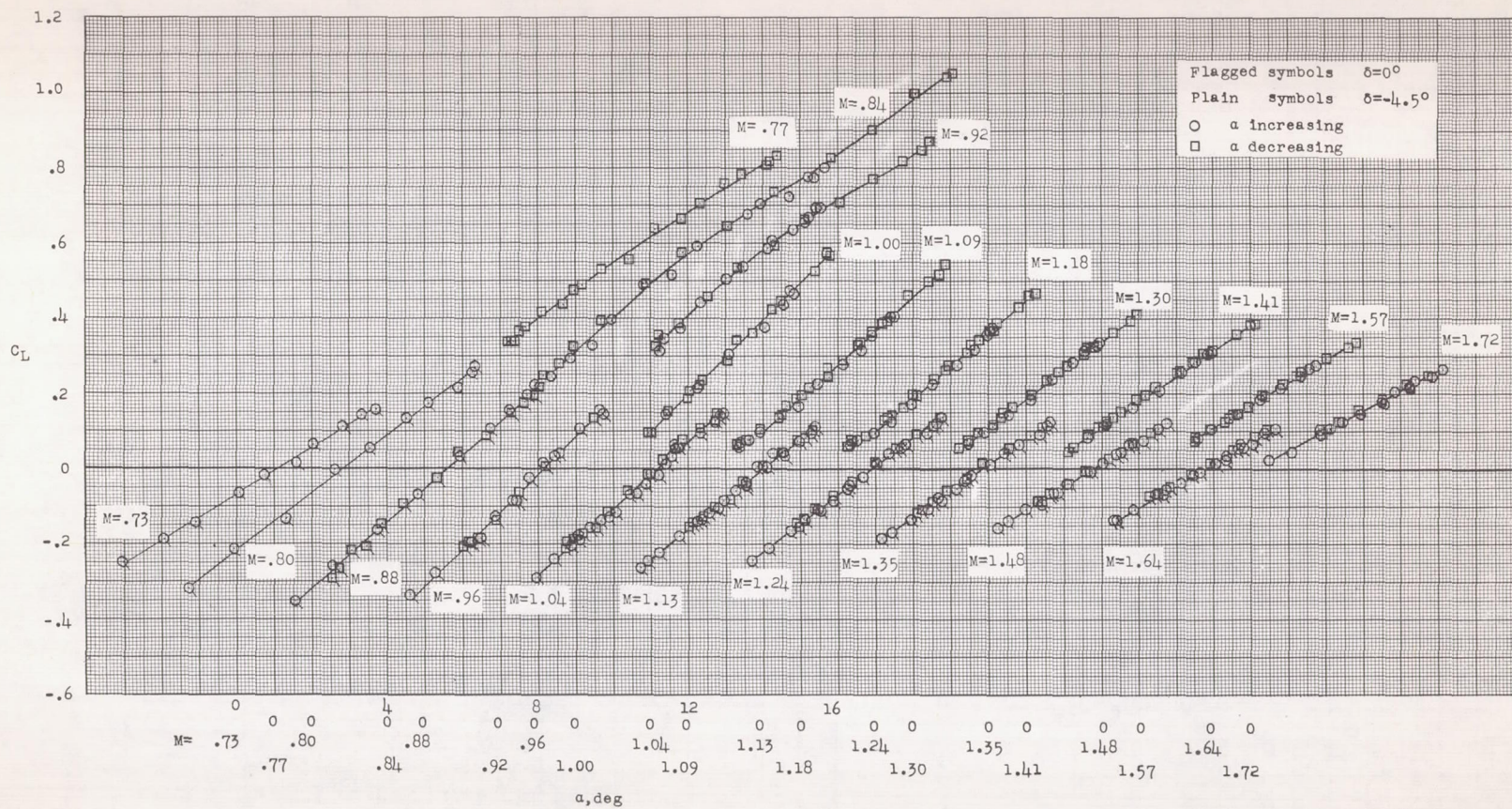
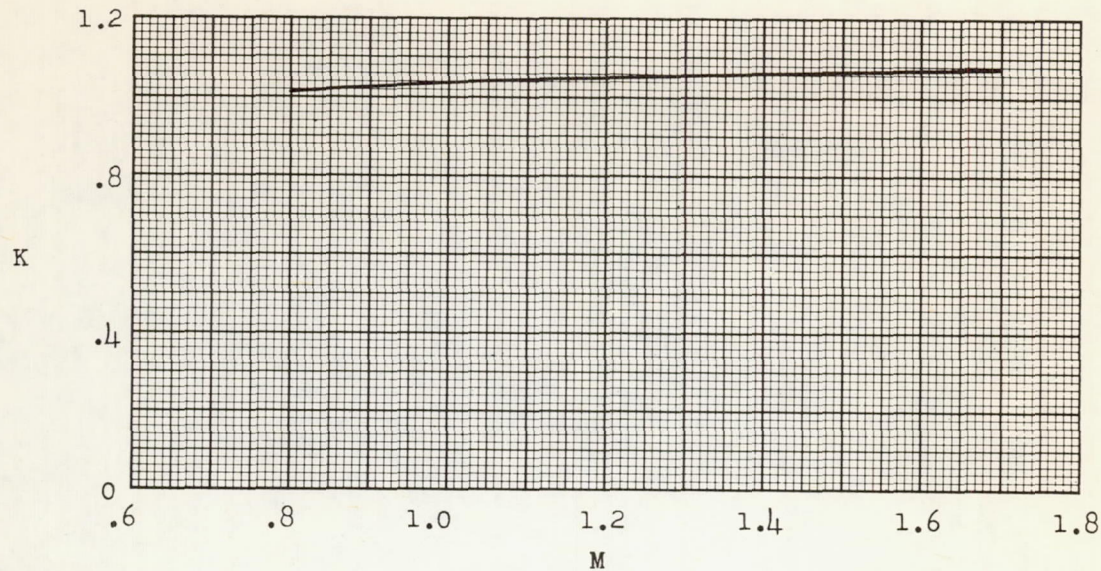
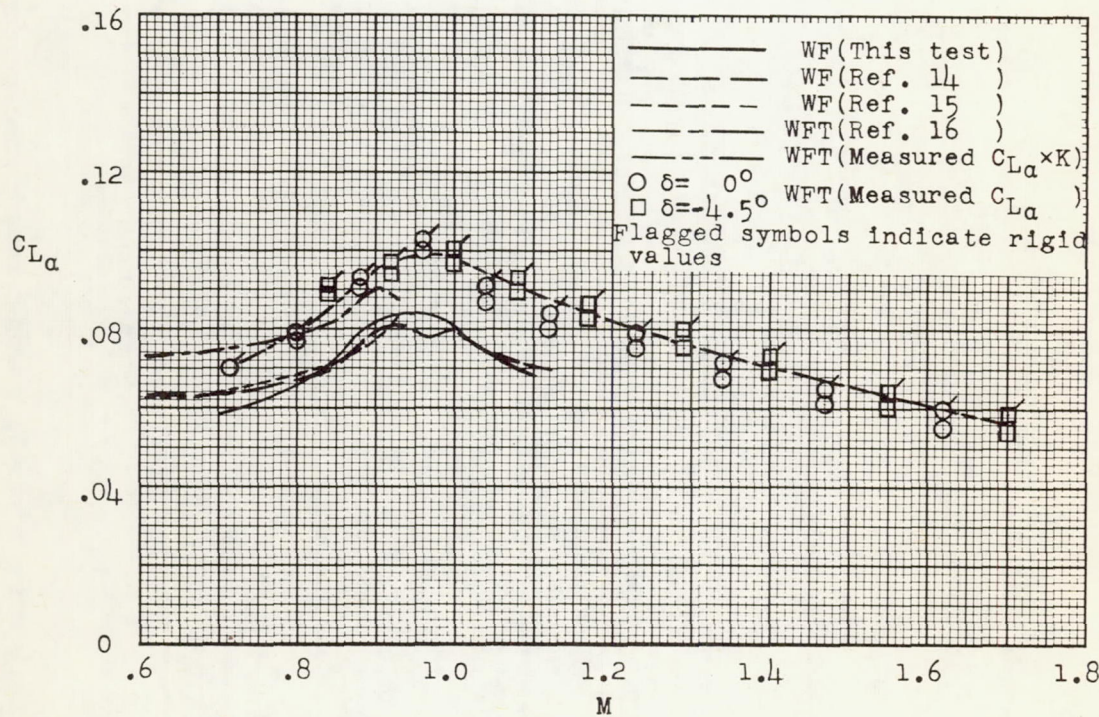


Figure 7.- Lift coefficient plotted against angle of attack for various Mach numbers and two tail settings.



(a) Factor for converting measured lift-curve slope to rigid wing values
where $(C_{L\alpha})_{\text{rigid}} = K(C_{L\alpha})_{\text{measured}}$.



(b) Measured lift-curve slope with wind-tunnel comparisons.

Figure 8.- Variation of measured lift-curve slope with Mach number and comparisons with wind-tunnel data.

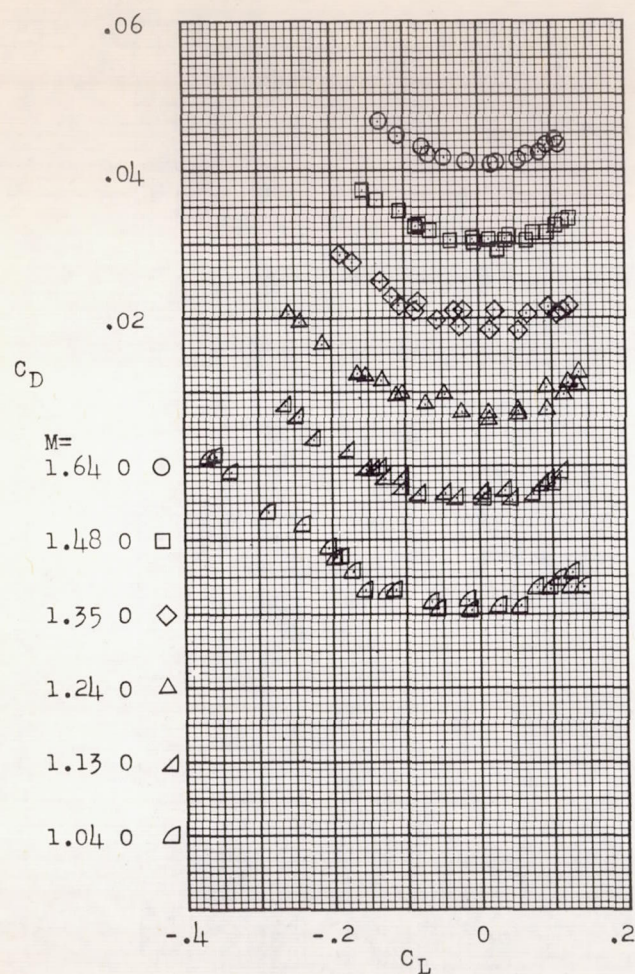
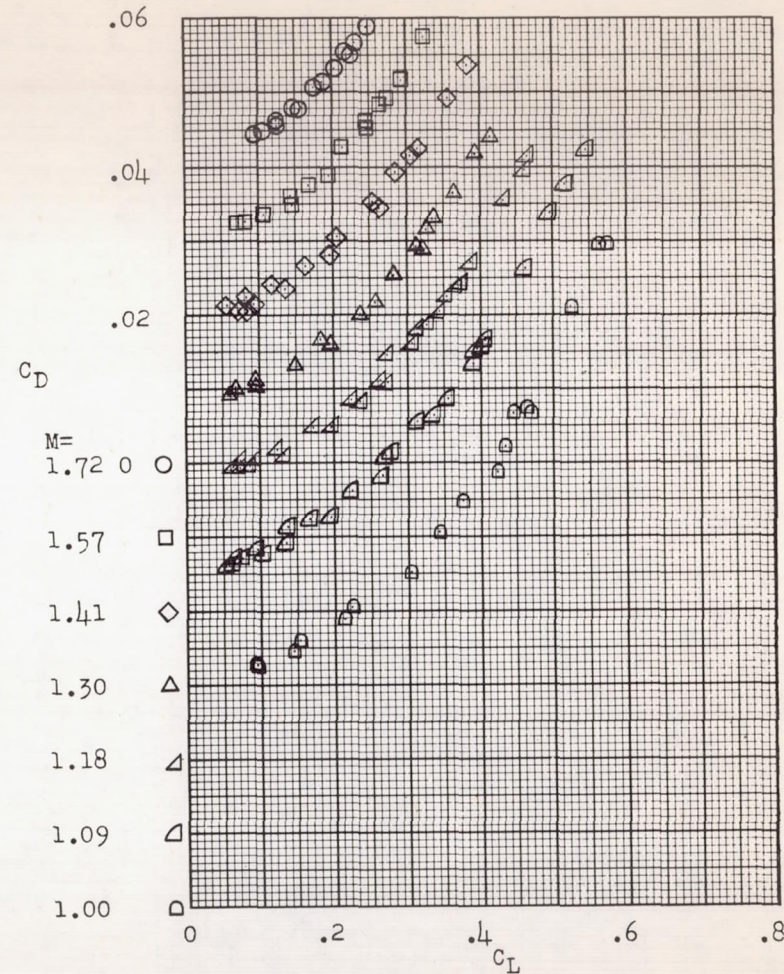
(a) $\delta = 0^\circ$.(b) $\delta = -4.5^\circ$.

Figure 9.- Drag coefficient as a function of lift coefficient for various Mach numbers and two tail settings.

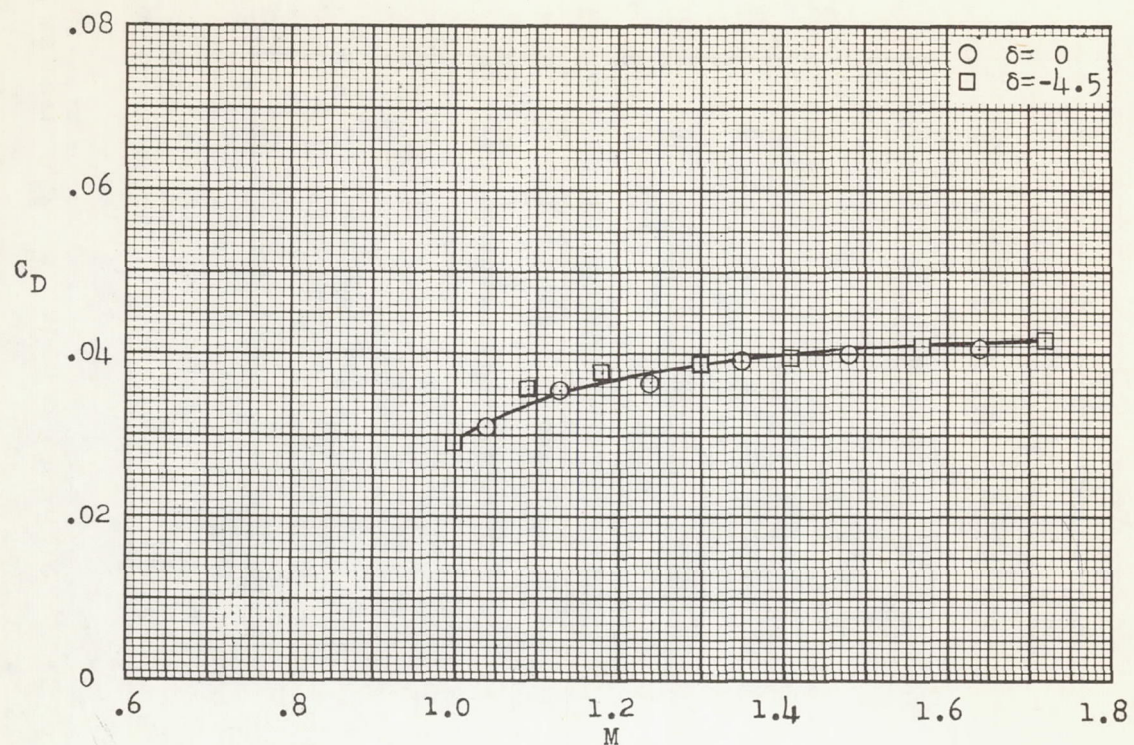


Figure 10.- Variation of minimum drag coefficient with Mach number.

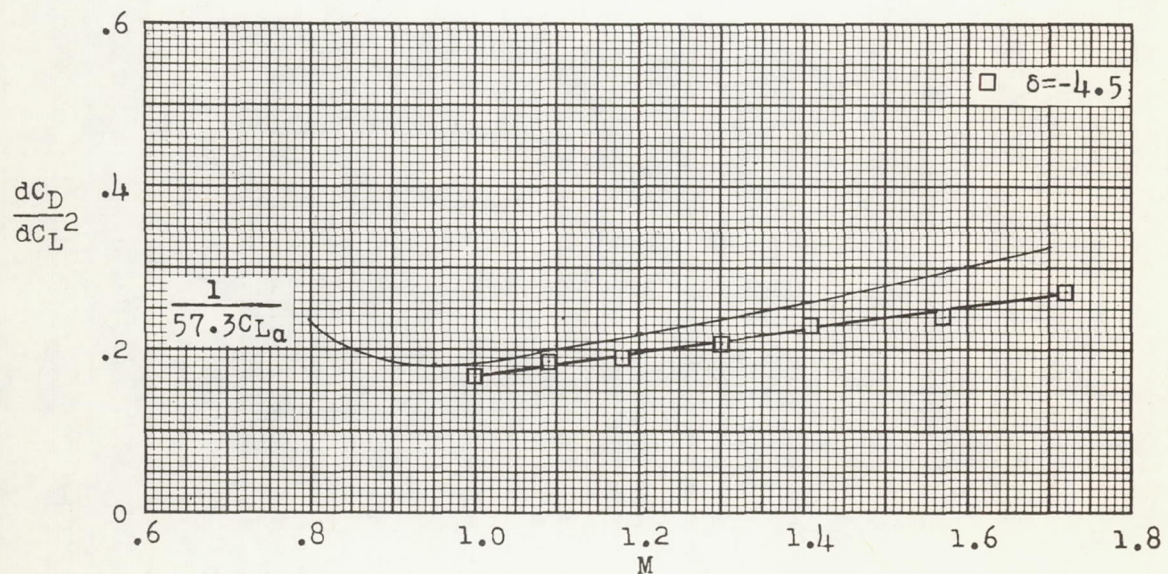


Figure 11.- Drag-due-to-lift parameter plotted against Mach number and comparison with zero leading-edge suction.

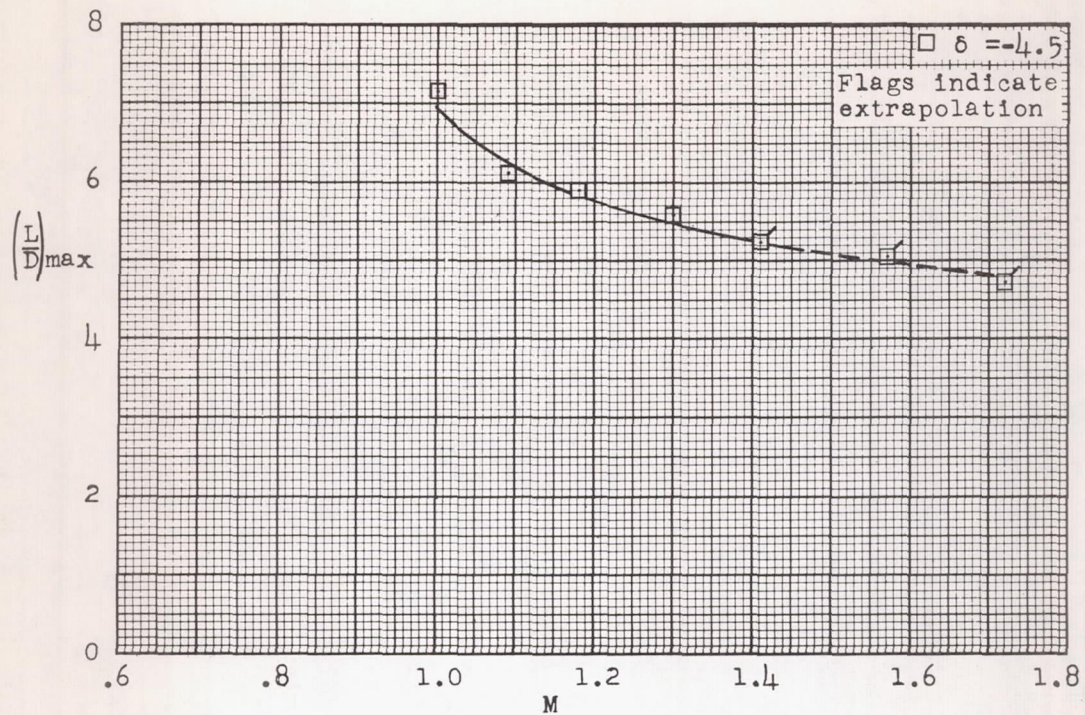


Figure 12.- Variation of maximum lift-drag ratios with Mach number.

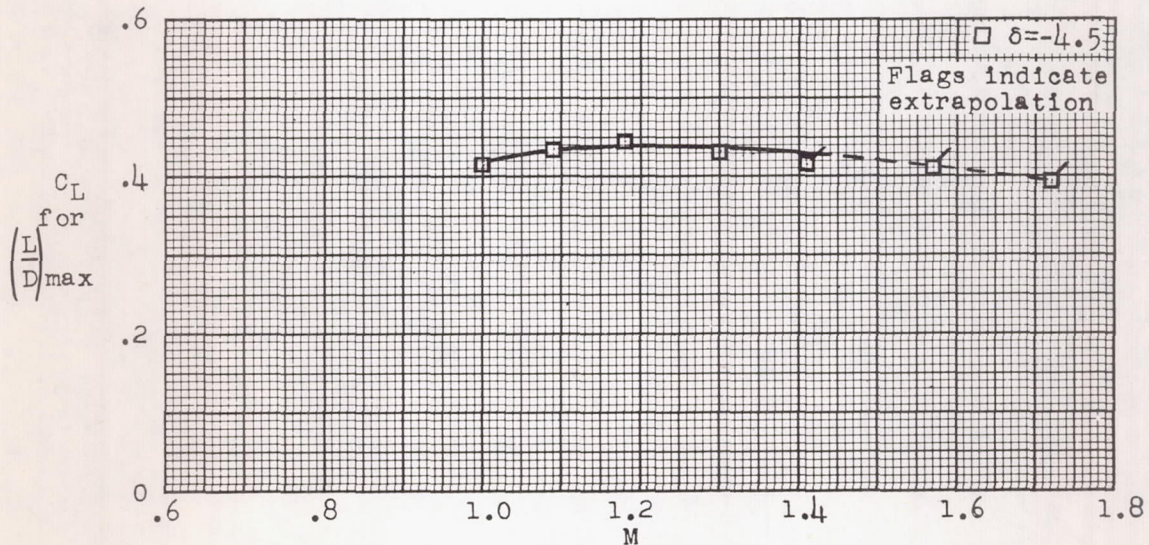


Figure 13.- Lift coefficient for maximum lift-drag ratios for various Mach numbers.

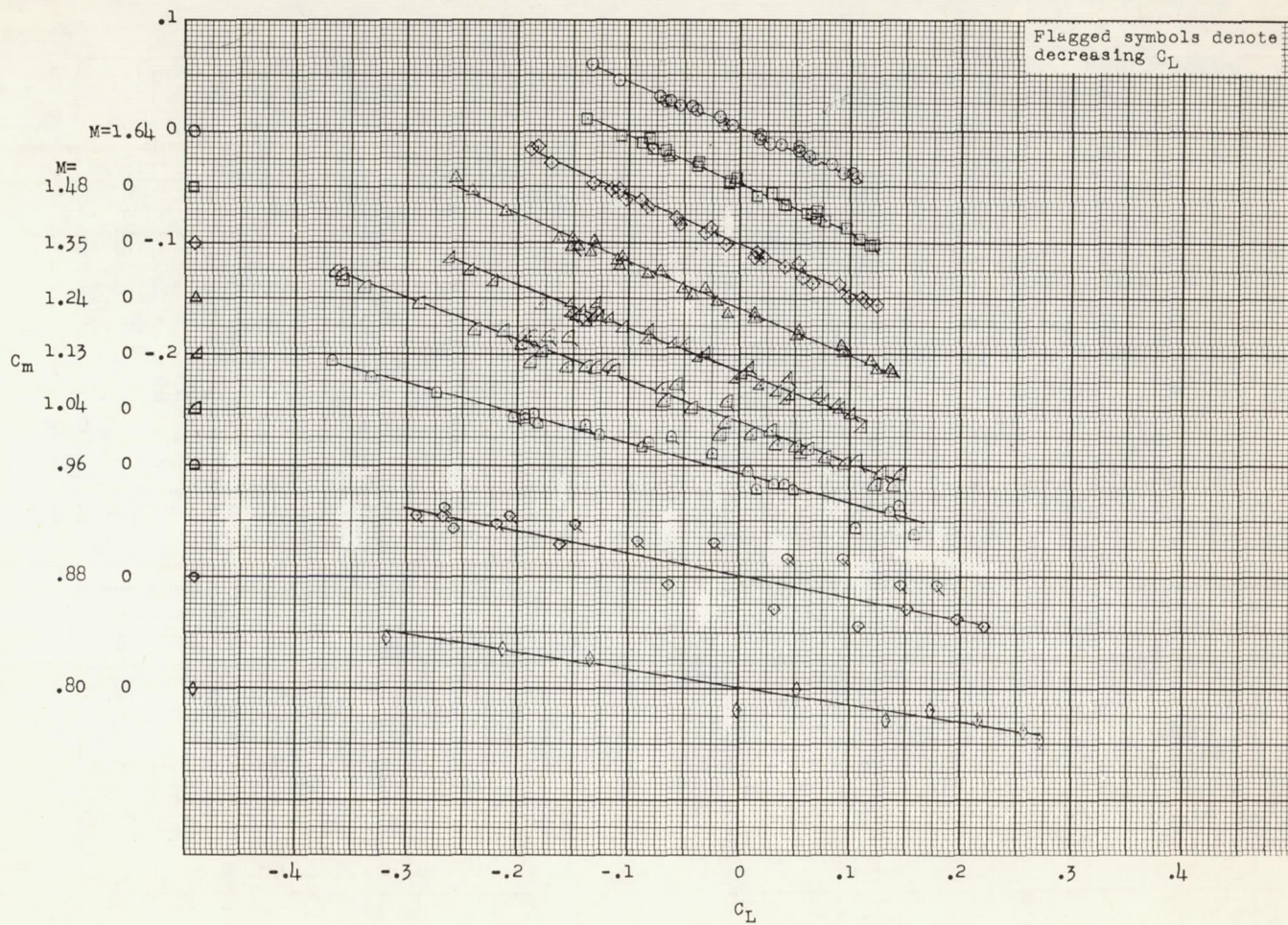
(a) $\delta = 0^\circ$.

Figure 14.- Pitching moment as a function of lift coefficient for various Mach numbers and two tail settings.

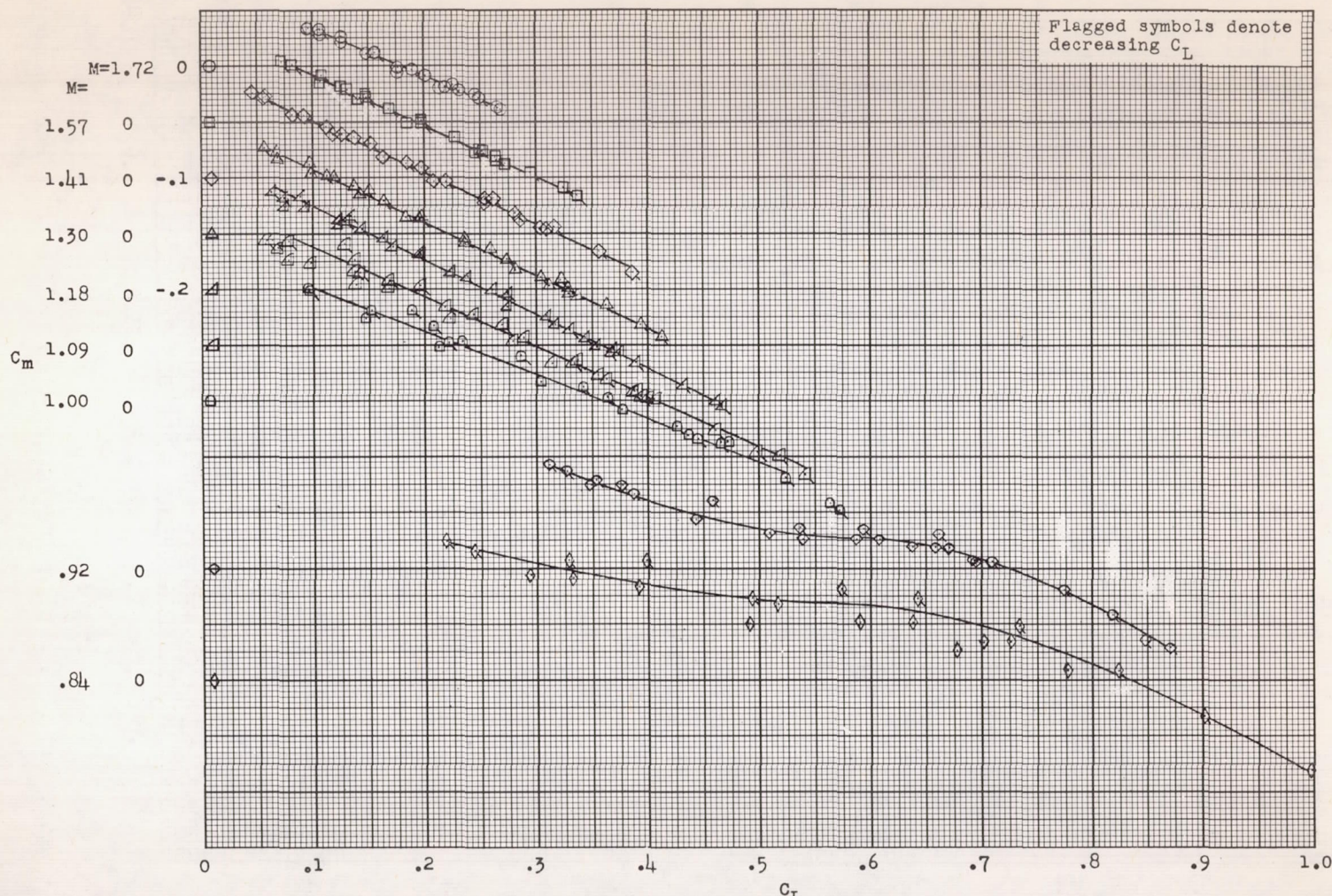
(b) $\delta = -4.5^\circ$.

Figure 14.- Concluded.

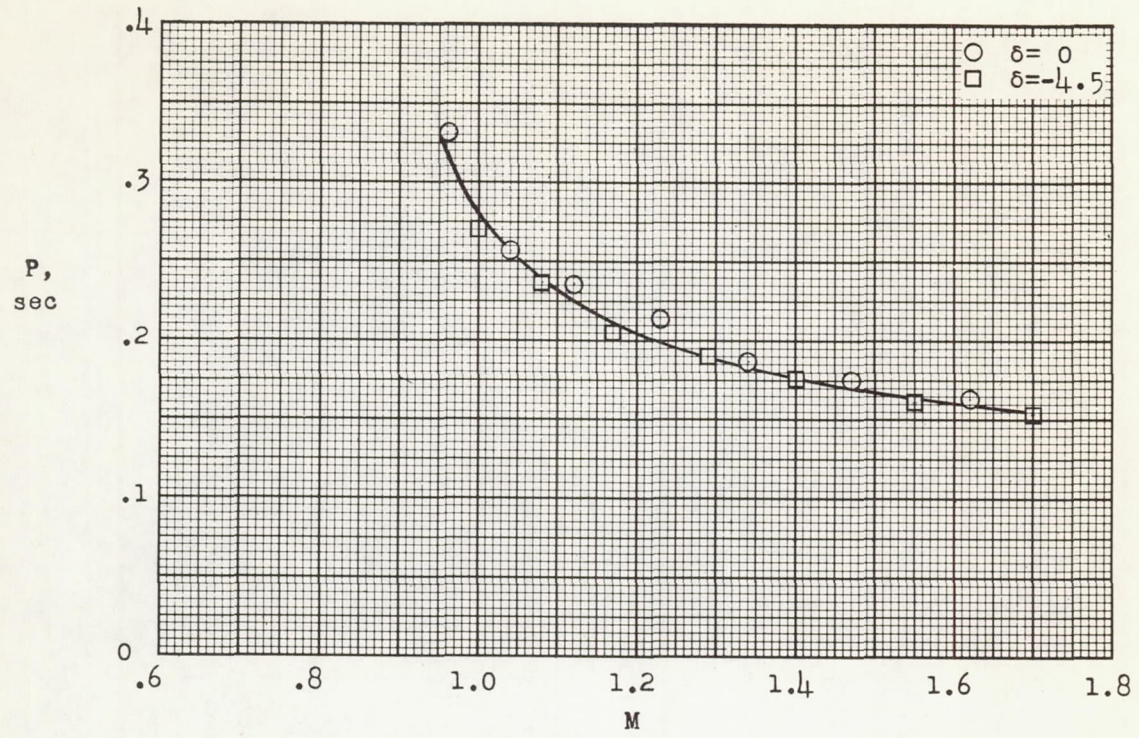


Figure 15.- Measured period of the pitch oscillation at various Mach number.

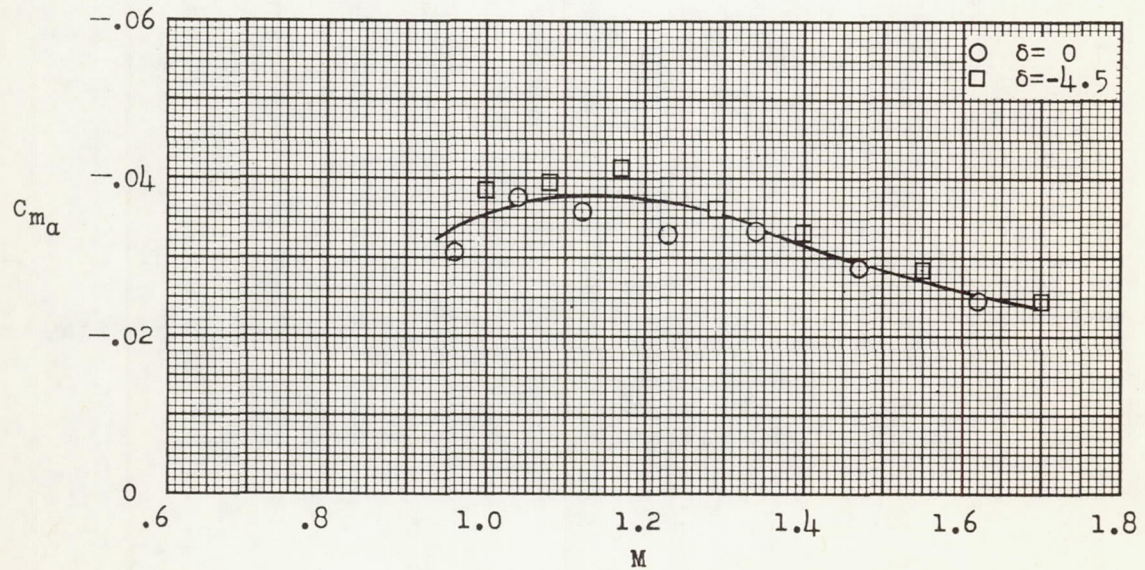


Figure 16.- Variation of the pitching-moment-curve slope with Mach number.

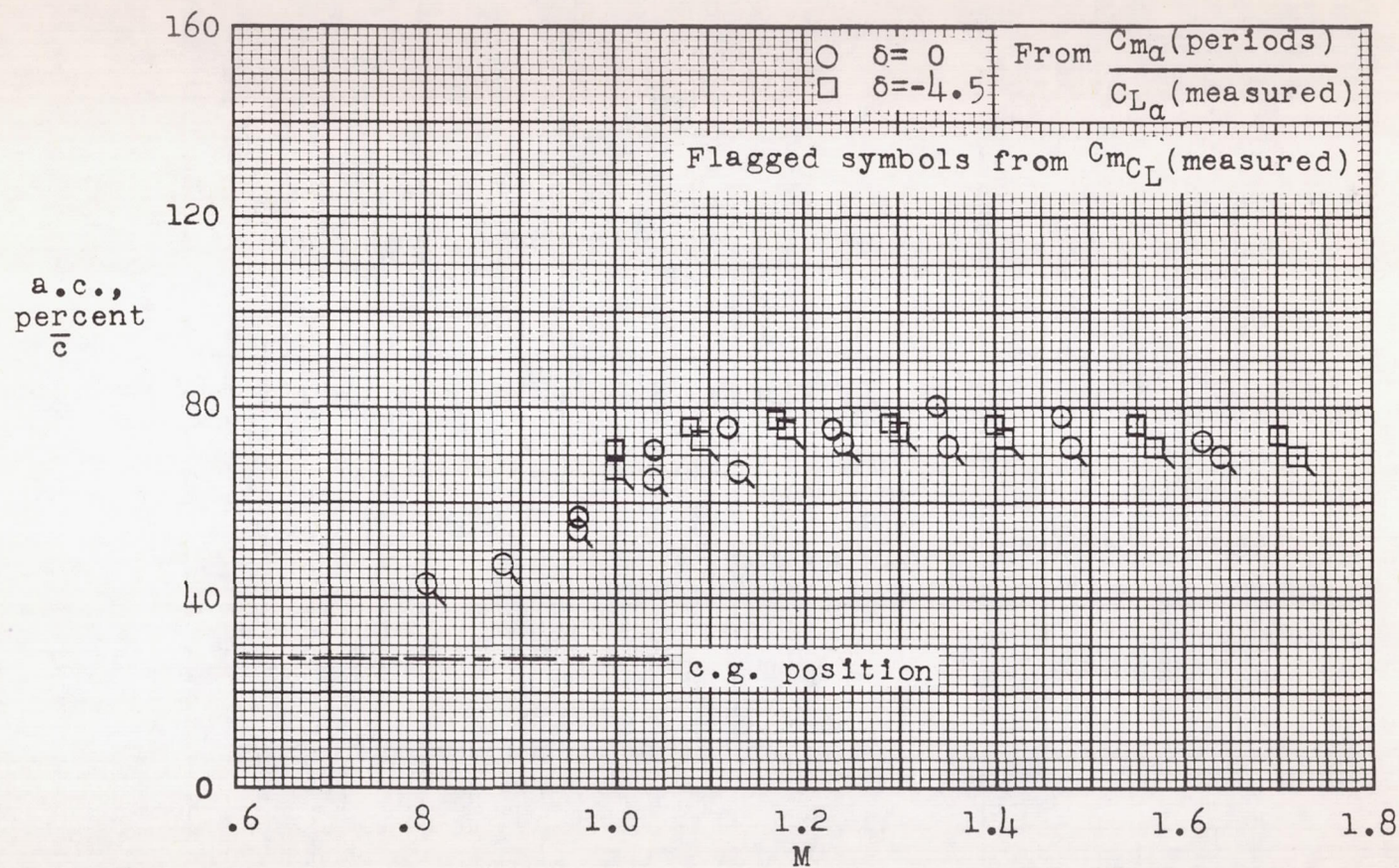
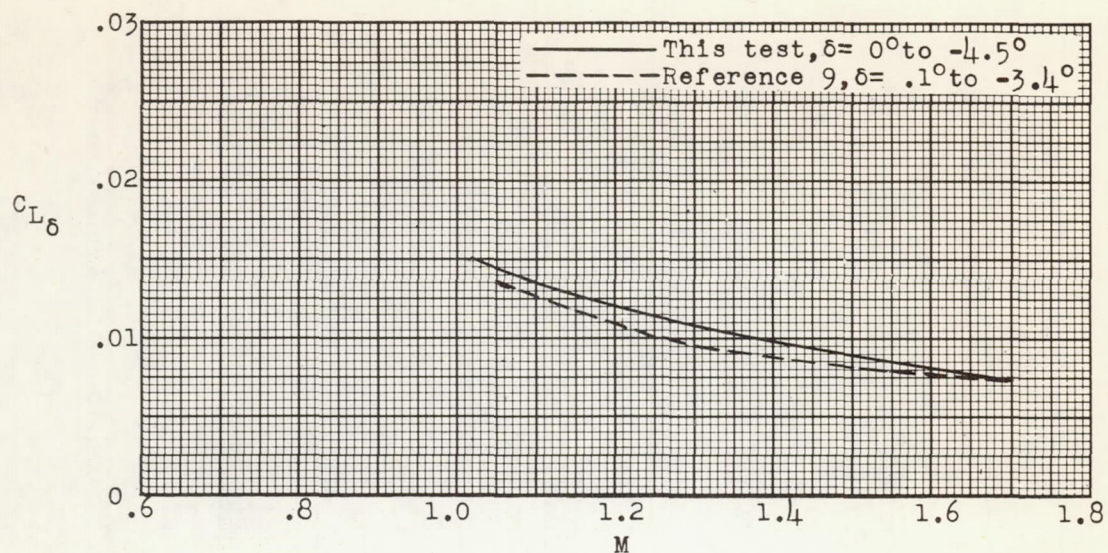
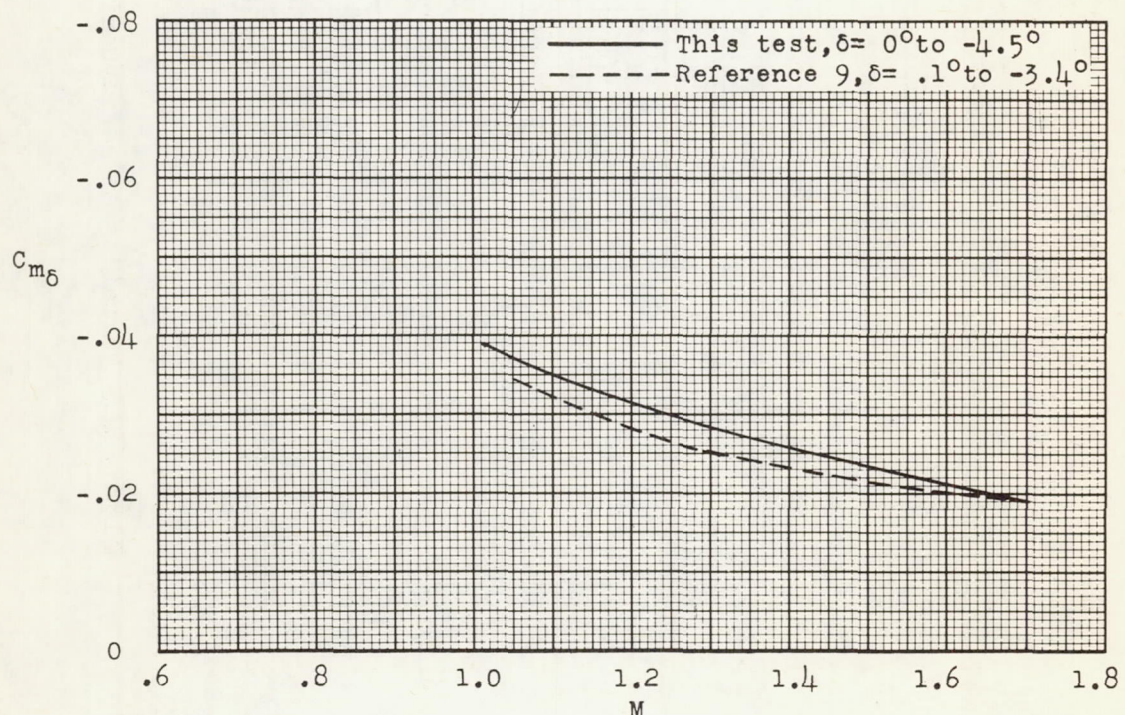


Figure 17.- Variation of aerodynamic-center position with Mach number.



(a) Effectiveness of the horizontal tail in producing lift.



(b) Effectiveness of the horizontal tail in producing pitching moment.

Figure 18.- Effectiveness of the horizontal tail in producing lift and pitching moment at several Mach numbers.

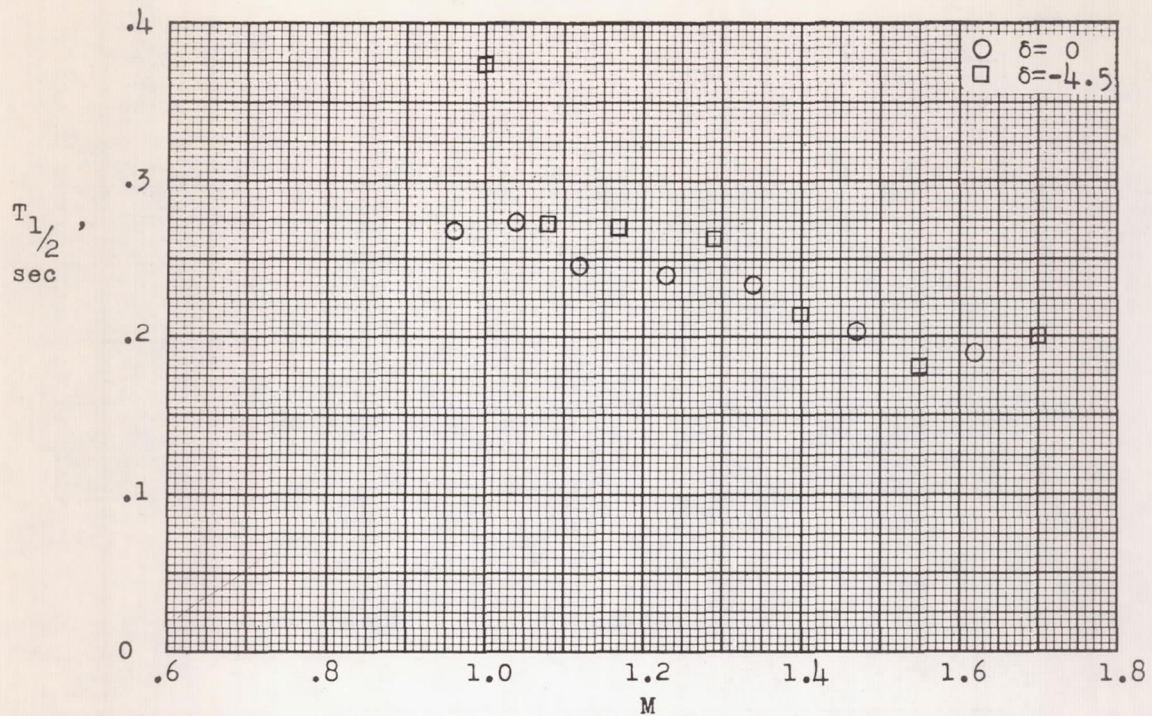


Figure 19.- Time for the pitch oscillation to damp to one-half amplitude as a function of Mach number.

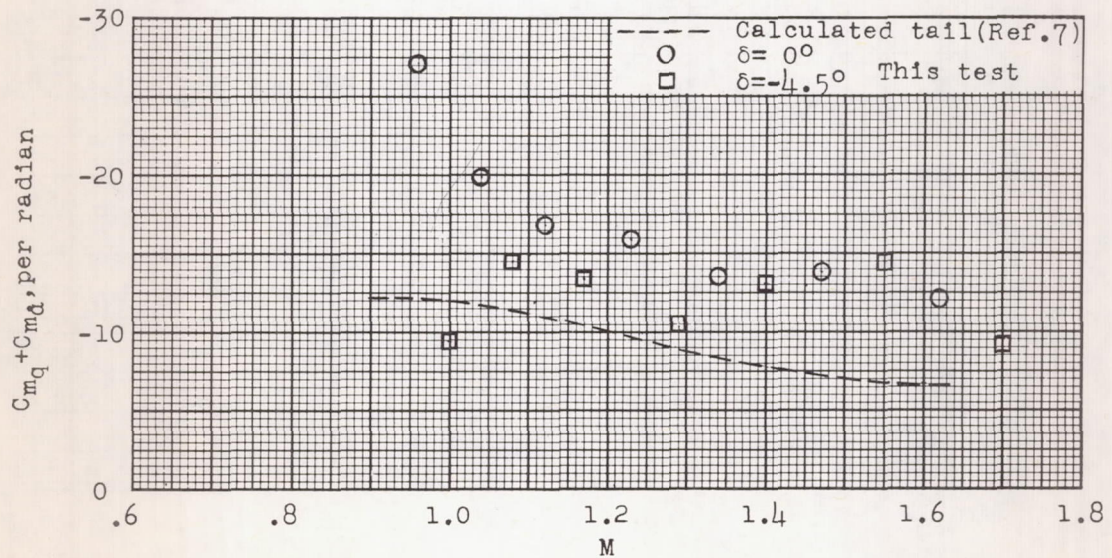


Figure 20.- Variation of the sum of the pitch-damping coefficients with Mach number.

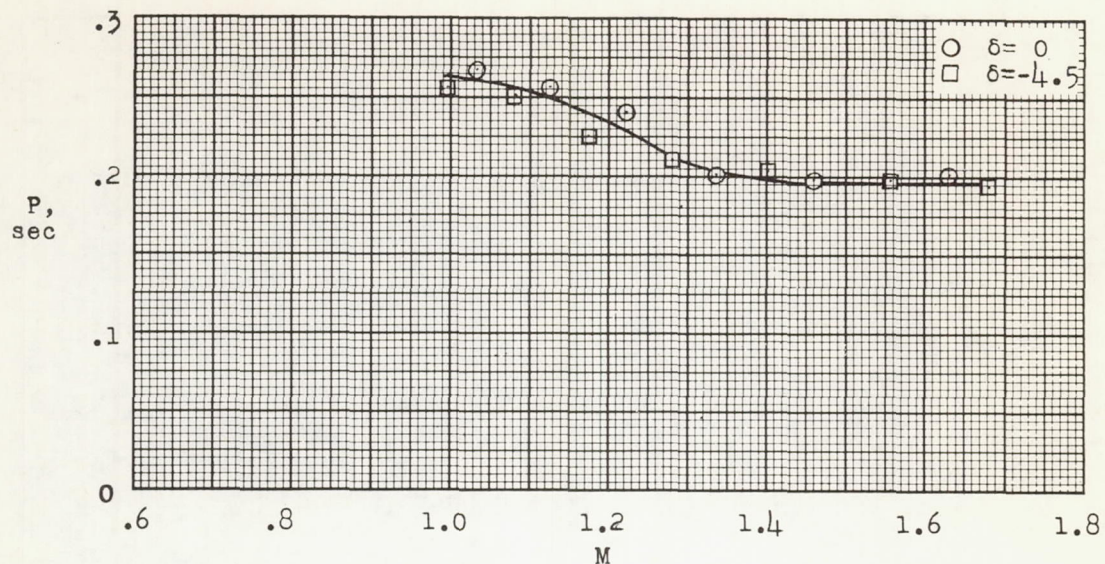


Figure 21.- Period of the oscillation in sideslip for various Mach numbers.

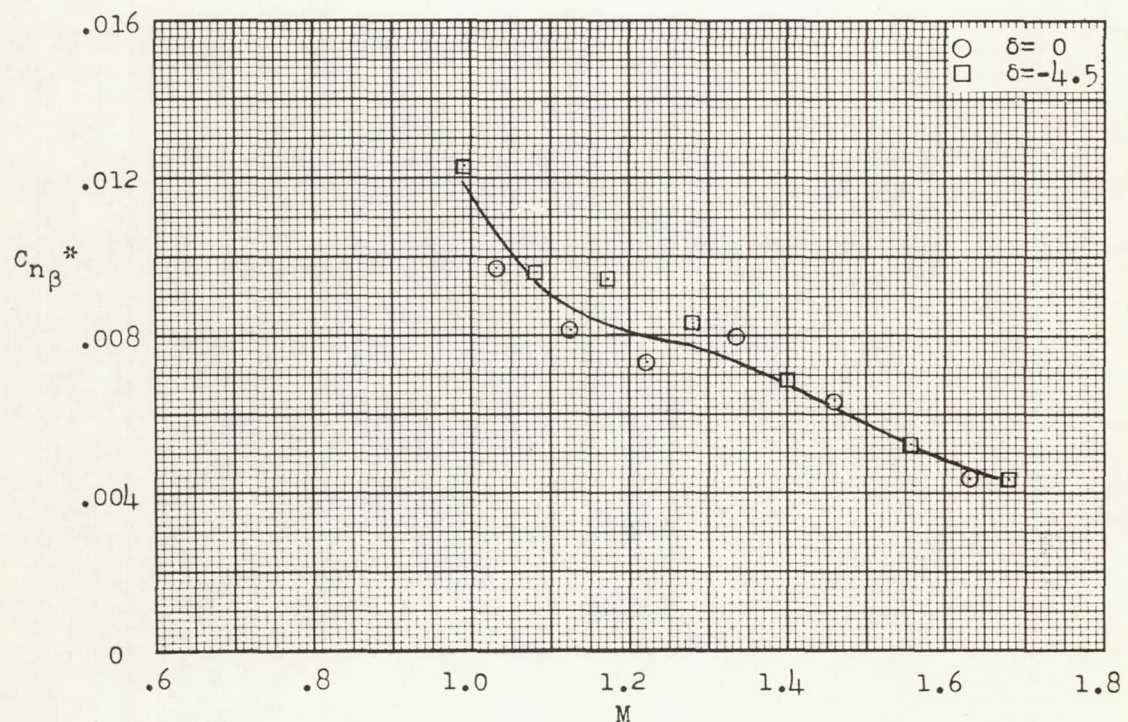


Figure 22.- Variation of static directional stability derivative $C_{n\beta}^*$ with Mach number.